A&A 456, 269–282 (2006)
DOI: 10.1051/0004-6361:20054011

Astronomy & Astrophysics

Non-gray rotating stellar models and the evolutionary history of the Orion Nebular Cluster

N. R. Landin[1,2], P. Ventura[2], F. D'Antona[2], L. T. S. Mendes[1,3], and L. P. R. Vaz[1]

[1] Depto. de Física, Universidade Federal de Minas Gerais, CP 702, 30161-970 Belo Horizonte, MG, Brazil
e-mail: [nlandin;lpv]@fisica.ufmg.br
[2] Osservatorio Astronomico di Roma, via Frascati 33, 00040 MontePorzio Catone, Italy
e-mail: [ventura;dantona]@mporzio.astro.it
[3] Depto. de Engenharia Eletrônica, Universidade Federal de Minas Gerais, CP 702, 30161-970 Belo Horizonte, MG, Brazil
e-mail: luizt@cpdee.ufmg.br

Received 8 August 2005 / Accepted 12 May 2006

ABSTRACT

Context. Rotational evolution in the pre-main sequence is described with new sets of pre-MS evolutionary tracks including rotation, non-gray boundary conditions (BCs) and either low (LCE) or high convection efficiency (HCE).
Aims. Using observational data and our theoretical predictions, we aim at constraining (1) the differences obtained for the rotational evolution of stars within the ONC by means of these different sets of new models; (2) the initial angular momentum of low mass stars, by means of their templates in the ONC.
Methods. We discuss the reliability of current stellar models for the pre-MS. While the 2D radiation hydrodynamic simulations predict HCE in pre-MS, semi-empirical calibrations either seem to require that convection is less efficient in pre-MS than in the following MS phase (lithium depletion) or are still contradictory (binary masses). We derive stellar masses and ages for the ONC by using both LCE and HCE.
Results. The resulting mass distribution for the bulk of the ONC population is in the range 0.2−0.4 $M_{\odot}$ for our new non-gray models and, as in previous analyse, in the range 0.1−0.3 $M_{\odot}$ for models having gray BCs. In agreement with Herbst et al. (2002) we find that a large percentage (∼70%) of low-mass stars ($M \lesssim 0.5\ M_{\odot}$ for LCE; $M \lesssim 0.35\ M_{\odot}$ for HCE) in the ONC appears to be fast rotators ($P < 4$ days). Three possibilities are open: 1) ∼70% of the ONC low mass stars lose their disk at early evolutionary phases; 2) their "locking period" is shorter; 3) the period evolution is linked to a different morphology of the magnetic fields of the two groups of stars. We also estimate the range of initial angular momentum consistent with the observed periods.
Conclusions. The comparisons made indicate that a second parameter is needed to describe convection in the pre-MS, possibly related to the structural effect of a dynamo magnetic field.

Key words. stars: evolution – stars: interiors – stars: rotation – stars: Hertzsprung-Russell (HR) and C-M diagrams

1. Introduction

We compute new sets of pre-MS models with the ATON code for stellar evolution, the version presented in Mendes et al. (1999), which includes stellar rotation according to the description by Endal & Sofia (1976), updated for the present work to employ non-gray boundary conditions by Allard & Hauschildt (1997) and Allard et al. (2000).

Our main goal is to improve our understanding of the appropriate physical constraints to be used for a general description of the evolution of stellar structure and its angular momentum with time. We are particularly interested on the choice of the stellar initial angular momentum and its variation with time, and, also, on the importance of convection efficiency during the pre-main sequence. To do this, we check our choices with respect to sets of relevant observations.

Since the pioneering work by Henyey et al. (1955) and Hayashi (1961) it is commonly accepted that pre-MS stars derive their luminosity by gravitational contraction, with the only exception of the short deuterium burning phase. Derivation of masses of young stellar associations has then generally been made by standard hydrostatic stellar models including deuterium burning, an approach that we will use in this paper. This procedure rests on the assumption that neither the residual accretion after the protostellar phase nor the uncertainty in the zero point of ages affect the results in a strong way.

Nevertheless, the theoretical description of moderately low and low mass objects is affected by the first principle uncertainties in the description of some physical inputs, in particular opacities, convection, equation of state (D'Antona 1993) and treatment of boundary conditions (BCs, Chabrier & Baraffe 1997). Since the low mass stars in the pre-MS are fully convective and over-adiabatic, any change in the convective model substantially alters the location of the track in the theoretical HR plane. The use of a less efficient treatment of convection leads to larger temperature gradients, so that, for a given luminosity, the structure readjusts on a more expanded configuration, with a consequent shift of the track to lower effective temperatures ($T_{\rm eff}$) (e.g. D'Antona & Mazzitelli 1994, 1997; D'Antona & Montalbán 2003). The path followed by the theoretical pre-MS tracks on the HR diagram is also dependent on the boundary conditions used to fit the numerical integration of the structural equations of the interior with the atmosphere. The use of a non-gray atmospheric treatment shifts the tracks to cooler $T_{\rm eff}$s within an extended interval of masses and ages (Montalbán et al. 2004). The effect due to the non-grayness of the atmosphere is, in many

cases, overwhelmed by the uncertainties related to the treatment of convection, that has a similar, but even stronger effect on the tracks, with only a few exceptions that are relevant for this work, as will be discussed in Sect. 6.3.

Young stellar clusters provide a unique opportunity to test stellar pre-MS models. Many studies in the past have been focused on the Orion Nebula Cluster (ONC), because it contains thousands of pre-MS objects. Hillenbrand (1997) measured the V and I magnitudes (and colors) of ∼900 stars and located them in the theoretical HR diagram by using bolometric corrections and taking into account the interstellar extinction for the determination of colors and bolometric magnitudes. In spite of the non-negligible uncertainties weighting on the derivation of these stellar parameters (Hillenbrand et al. 1997), such a work has been widely used, in connection with theoretical pre-MS tracks, to infer important information concerning the cluster itself. The mass and age distributions and the slope of the mass function can all be estimated by inferring the appropriate mass and age for each observed star. It is clear that the results obtained with this approach will depend to a certain extent on the set of tracks used to perform the analysis, and on the physical inputs adopted to calculate the evolution. This is confirmed by the fact that, specifically for the ONC, studies that used different sets of evolutionary tracks reached significantly different conclusions, particularly with respect to the mass and age distribution, and, more important, to the age spread and, consequently, to the evolutionary history of the star formation process within the cluster (Palla & Stahler 1999).

In the past few years, new detailed observational studies of the ONC have been undertaken, focused on the rotational properties of the stars. Stassun et al. (1999) and Herbst et al. (2002) measured the rotational periods of ∼400 stars belonging to the ONC. All of them are in the Hillenbrand (1997) sample, so they can be located on the HR diagram. More recently, Stassun et al. (2004) and Flaccomio et al. (2003a,b) reanalyzed all the archival *Chandra* observations of the ONC studying in great detail the X-ray properties of the observed objects, in an attempt to elucidate the origin of X-ray emission in pre-MS stars. All this available information renders the ONC an excellent laboratory to test stellar evolution theories of the pre-MS phase.

None of the previous analyses of the ONC rotational database has been done using non-gray models, and the effect of using different convection efficiencies has not been extensively tested. We therefore decided to use this database to test and calibrate our new sets of non-gray tracks for rotating stellar models, with masses in the range $0.085 \leq M/M_{\odot} \leq 3.8$. As a byproduct, we will have insight on how much the rotational properties of this population depend on the choice of the evolutionary tracks. At present, there is no definitive observational constraint that can be used to choose among the tracks obtained by using different convection inputs. In this work we derive masses and ages with different sets, in order to appreciate how much the results we are presently interested in, namely those on the angular momentum evolution, depend on the choice. In particular, we will test the role of (a) boundary conditions (gray and non-gray), (b) different convection efficiencies in the framework of the MLT, and (c) rotating and non-rotating models.

As indicated by the non-negligible differences among the set of tracks adopted, we show that the detailed period distribution as a function of mass and age is dependent on the physical inputs. However, the qualitative information on the rotational distribution of stars of different mass in the ONC remains similar, and we confirm that the distribution of periods is bimodal only for masses larger than a "transition" mass depending on the convection model.

In Sect. 2 we summarize the uncertainties in the theoretical models, and also try to clarify some issues left ambiguous in the recent literature on pre-MS evolution. In Sect. 3 we provide a brief description of the latest rotational, non-gray version of the ATON stellar evolution code, and describe the choice of the main physical and chemical inputs used for the present work in Sect. 4. The role played by the convective modeling on the location of pre-MS tracks on the HR diagram, the role played by non-grayness, and the lithium pre-MS depletion are discussed in Sect. 5. In Sect. 6 we present the photometric and rotational data related to the ONC stellar population, and the derivation of masses and ages from our new sets of tracks. The results on the rotation period distribution and its possible interpretation(s) are discussed in Sect. 7. Conclusions are given in Sect. 8.

2. Uncertainties in the standard hydrostatic stellar models

We briefly rewiew the reliability of the procedure of deriving ages and masses of young stellar population based on hydrostatic evolutionary tracks. We first discuss two preliminary important physical points: (1) Is it appropriate to neglect residual accretion from the disk? (2) As the models disregard the hydrodynamic formation process, how do we take into account the zero point of ages? We summarize the well known uncertainties in the location of evolutionary tracks in the HR diagram and show why current data do not allow us to choose among models.

2.1. The role of residual accretion

The pre-MS phase begins after the main accretion phase, during which the protostellar core is formed and the star is embedded into the dust of the forming cloud. When objects of low mass become luminous in the visible or near infrared bands, the main accretion phase can be considered finished, although the accretion disk is still present in many cases. Accretion then will not change the final stellar mass much, while the presence of the accretion disk may be very important in determining the rotational evolution of the star. In the pre-MS, accretion still may occur at rates in the range $\sim 3 \times 10^{-9}$–4×10^{-7} $M_{\odot}$/yr (Basri & Bertout 1989) for classical T Tauri (TT) star, and mostly below $\sim 10^{-10}$ $M_{\odot}$/yr for very low mass stars below ∼0.2 $M_{\odot}$ (Mohanty et al. 2005). Walter (1987) and Strom et al. (1989) noticed the coexistence of classical and weak TT stars in the same region of the HR diagram, corresponding to an age range (derived from standard hydrostatic models without accretion) from $\sim 3 \times 10^5$ yr to $\sim 3 \times 10^6$ yr, concluding that the disk evolution is decoupled from the evolution of the central star, and that the disk may disappear either early or at late stages. This will affect the stellar rotation in different ways, as shown by subsequent studies (e.g. Bouvier et al. 1993), interpreted in terms of magnetic disk locking (Bouvier et al. 1997).

Can the residual mass accretion alter the stellar evolution? Deuterium burning from the accreted matter provides a luminosity $L \sim 15\ L_{\odot} \times (\dot{M}/(10^{-5}\ M_{\odot}/\mathrm{yr}))$ (Stahler 1988), which could influence the evolution only for very high rates of mass accretion, or at very low luminosity. Accretion itself may alter the evolution if the accretion timescale $M/\dot{M}_{\mathrm{crit}}$ is of the order of the thermal (Kelvin-Helmholtz) timescale t_{KH}. At high luminosity, where $t_{\mathrm{KH}} \sim 10^5$ yr for a typical TT, this constraint is not respected only for very high accretion rates. At about the solar

luminosity $t_{\rm KH} \sim 2 \times 10^6$ yr, for which $\dot{M}_{\rm crit} \sim 5 \times 10^{-7}\ M_\odot$/yr, which is at the upper boundary of the values observed in TT. In this case, or in similar cases, the evolution can be altered, but this $\dot{M}$ cannot be sustained for a very long time, otherwise we would not find low masses surviving. Thus we conclude that evolution in which accretion plays a dominant role, such as described e.g. by Hartmann et al. (1997) and Tout et al. (1999) may be relevant only for a short lifetime, in a small fraction of the pre-MS stars, and that the bulk properties of young stellar associations can be derived by adopting traditional pre-MS hydrostatic models.

2.2. The zero point of stellar ages

One other item that must be taken into account is the definition of the zero point of ages, which, for the hydrostatic pre-MS evolution, is connected to the location in luminosity of the "starting model", i.e. the internal thermodynamic conditions within the star when the mass accretion process ends. The uncertainty in the starting models is reflected in the age-luminosity relationship. A first uncertainty is due to the fact that we do not know whether the deuterium burning phase occurs during the visible pre-MS or during the main accretion phase: this depends on the average protostellar accretion rate (see D'Antona & Mazzitelli 1997 for a discussion). For the stars that do not completely burn deuterium in the protostellar phase ($M \lesssim 0.5\ M_\odot$), the typical uncertainty in the lifetime, however, must be of the order of $t_{\rm KH}$ at the end of the main accretion phase (e.g. Tout et al. 1999). In the model by Palla & Stahler (1990, 1993), in which the stellar core of low mass stars emerges at visible wavelengths close to the deuterium burning region in the HR diagram (birthline) due to the "thermostat" action of D-burning, the typical $t_{\rm KH}$ is the thermal timescale at the D-burning luminosity and radius, $\sim 10^5$ yr for masses of a few tenths of $M_\odot$, and up to $\sim 10^6$ yr for 0.1 $M_\odot$. For the lowest masses, however, the "birthline" concept may not be valid, as the main accretion phase may end before deuterium is ignited, and the stars probably start their hydrostatic evolution at higher luminosities, where the thermal timescale, and thus the uncertainty in the zero point of ages, would be smaller.

On the other hand, we must be careful not to confuse the "numerical" uncertainties with the "physical" uncertainties. Hydrostatic contraction will let the star ignite D-burning as soon as the central physical conditions allow it, and it seems very unlikely that we can take as a zero point of the pre-MS a model with central temperatures in the middle of the deuterium burning phase, disregarding the action of the thermostat[1].

2.3. The role of non-gray atmospheres

In the gray atmosphere approximation the increase of the temperature T from the surface moving inwards is described via a relationship between T and the optical depth (τ), and the pressure is calculated by integrating the hydrostatic equilibrium equation. The match between the interior and the external layers is made at $\tau = 2/3$. Any link between pressure and temperature in the atmosphere, fixed by the either a convective or radiative gradient, is ignored. In the non-gray treatment a self-consistent integration is performed down to an optical depth at which the diffusion approximation is valid (Morel et al. 1994), and including the treatment of atmospheric convection, which cannot be neglected at low $T_{\rm eff}$s. The use of frequency-dependent opacities may also modify the onset of convection within the atmosphere, and both the $T_{\rm eff}$ and the colors of the tracks can be strongly affected. The necessity of adopting outer boundary conditions based on realistic non-gray atmosphere models for the pre-MS and low mass MS was pointed out by Chabrier & Baraffe (1997; and references therein), who have shown that the use of radiative $T(\tau)$ relations or gray atmosphere models is invalid when molecules form near the photosphere, at $T_{\rm eff}$ below 4000 K. Outer boundary conditions based on the gray assumptions yield hotter models for a given mass. According to Baraffe et al. (1998) the use of an inappropriate outer boundary condition, such as the Eddington approximation, yields an overestimation of $T_{\rm eff}$ for a given mass up to 300 K.

2.4. The role of convection

There is broad consensus in the literature that the treatment of superadiabatic convection in the pre-MS affects the tracks location to a great extent. In a series of works focusing on understanding the role played by different physical inputs on the pre-MS evolution, D'Antona & Mazzitelli (1997), D'Antona & Montalbán (2003), and Montalbán et al. (2004) outlined the major impact of convection modeling on the location of the stellar tracks in the HR diagram. Convection was found to be by far the most relevant ingredient influencing the determination of the mass and age of observed stars.

When modeling convection, it is essential to specify the mixing scale Λ, i.e. the typical distance that convective eddies travel before dissolving and delivering their excess gravo-thermal heat to the environment. The role played by Λ is relevant for the determination of the temperature gradient, as the conservation of flux implies that a larger Λ must be compensated by a lower degree of overadiabaticity. The convective flux behaves as $F_{\rm C} \sim \Lambda^2$ in zones where most of the energy is carried by convection. Conversely, within low efficiency convective regions, $F_{\rm C} \sim \Lambda^8$. The impact of the choice of Λ is therefore more evident where convection is not efficient. The pre-MS tracks result to be particularly sensitive to convective modeling, because the surface convection extends to most of the (if not the whole) star, and the low densities involved (particularly in the early phases of gravitational contraction) make the convective process highly inefficient.

Presently, the main ways of computing convection in stellar envelopes, for wide grids of stellar models, are:

1. The traditional mixing length theory – MLT (Böhm-Vitense 1958, and subsequent variations of this same model) – assumes that both the dimension of the convective eddies and the mixing length are proportional to the local value of the pressure scale height, i.e. $\Lambda = \alpha H_{\rm p}$, where α is a free parameter that is usually calibrated in order to reproduce the solar radius.
2. In the Full Spectrum of Turbulence model – FST (Canuto et al. 1996) – the whole spectrum of eddies' dimensions is

[1] Some models of the widely adopted grids by Baraffe et al. (1998) begin their evolution at a luminosity in the middle of D-burning, which lasts for $\sim 2 \times 10^6$ yr at 0.1 $M_\odot$. This is due to the fact that the lowest available gravity in the NextGen (Allard & Hauschildt 1997, AH) atmospheric grid, which these models employ, was $\log g = 3.5$. The more recent models by Baraffe et al. (2002) start at lower gravity, and reach the D-burning luminosity by contracting in thermal equilibrium. Of course, in these two sets of models the temporal evolution of luminosity is very different for the first $\sim 2 \times 10^6$ yr, but this does not automatically mean that this figure is the physical uncertainty in the ages, as the "numerical" choice of starting from a model with central temperature in the middle of the D-burning stage does not necessarily correspond to a physically plausible behavior (Montalbán & D'Antona 2006).

considered, and the mixing length is taken as the distance of the nearest convective border.
3. MLT, in which the α value for each gravity and $T_{\rm eff}$ is calibrated upon 2D or 3D hydrodynamical simulations.

Ludwig et al. (1999), using their 2D radiation hydrodynamic models, have provided a calibration of the parameter α in a wide region of $T_{\rm eff}$'s and gravities[2] to be used in the computation of *gray* stellar models. These 2D models indicate that convection in the pre-MS is on average more "efficient" than in the MS, corresponding to a larger α. The idea of calibrating the average α using numerical simulations has been extended by now to a few 3D computations: Ludwig et al. (AHS, 2002), for an M dwarf at $T_{\rm eff} = 2800$ K and $\log g = 5$, find $\alpha \simeq 2.1$; and Trampedach et al. (1999), for the range of main sequence gravities and $\log T_{\rm eff} = 3.68$–3.83, find $\alpha \simeq 1.6$–1.8 in the whole range. Asplund et al. (2000) have compared 2D and 3D atmosphere models for Sun, and found that the 2D solar model has marginally larger gradients than the 3D one. Although an extrapolation to regions not explicitly computed is not allowed, also these few 3D models indicate efficient convection in the overadiabatic envelope. Montalbán & D'Antona (2006) have computed gray models by using this calibration: the tracks they obtain are very similar to the FST tracks[3]. Unfortunately, a very efficient convection in pre-MS is *not* consistent with the lithium depletion patterns of young open clusters (D'Antona & Montalbán 2003). Any attempt to calibrate convection efficiency in pre–MS by means of comparisons between binary masses dynamically determined and those assigned from different sets of evolutionary tracks (HCE and LCE), seems to be ambiguous (Landin et al. 2006).

2.5. The role of convection coupled with non-gray atmospheres

We note a point that is generally overlooked, but that is crucial in order to understand the relevant parameters in track building: Montalbán et al. (2004) have shown that the problem of convection is intertwined in a subtle way with the problem of non-gray boundary conditions. For example, in the MLT framework, convection in the pre-MS should be described not only by the ratio $\alpha = l/H_{\rm p}$ in the interior of the star ($\alpha_{\rm in}$), below the non-gray atmosphere, but also by the value that this parameter has in the atmosphere itself ($\alpha_{\rm atm}$), and by the matching point between atmosphere and interior ($\tau_{\rm ph}$). In particular, the two widely used sets of model atmosphere by Baraffe et al. (1998) are referred to as the set built with $\alpha = 1.9$ and the set having $\alpha = 1.0$. Thus they are supposed to provide a clue to how the tracks vary by changing from a moderately high convective efficiency (HCE) represented by the set $\alpha = 1.9$, to a low convection efficiency (LCE) represented by the set $\alpha = 1$. However, in Baraffe et al. (1998), the parameter α refers only to the value of $\alpha_{\rm in}$, and is misleading for two reasons: (1) the set $\alpha_{\rm in} = 1.9$ stops at masses $M \geq 0.6\ M_{\odot}$, and only the set $\alpha_{\rm in} = 1.0$ is available for masses $M < 0.6\ M_{\odot}$; (2) for both sets, the atmospheric model grid adopted is the same, and computed with $\alpha_{\rm atm} = 1.0$. Montalbán et al. (2004) have shown that the fact that most of the superadiabatic part of the envelope is computed with a very inefficient convection ($\alpha_{\rm atm} = 1.0$) shifts the $T_{\rm eff}$ by $\sim$−150 K for the solar pre-MS. Thus one may be led to attribute the smaller $T_{\rm eff}$s of the Baraffe et al. (1998) tracks to the use of the non-gray atmospheres, whereas they are due in part to the fact that these non-gray atmospheres are computed with LCE.

3. Rotating stellar models

The pre-MS tracks were calculated by means of the ATON stellar evolution code. A full and detailed description of the numerical structure can be found in Mazzitelli (1989) and Mazzitelli et al. (1995). Here we briefly recall the main micro- and macrophysics input.

3.1. Rotation

As described in Mendes et al. (1999) rotation was implemented in the ATON code according to the approach followed by Endal & Sofia (1976), which uses the Kippenhahn & Thomas (1970) method improved with a potential function that includes a term related to the distortion of the figure of the star. In this approach the spherical surfaces used in standard stellar models are replaced by the equipotential surfaces.

The current version of the code allows one to choose among three rotational schemes:

- rigid body rotation throughout the whole star;
- local conservation of angular momentum in the whole star;
- local conservation of angular momentum in radiative regions plus rigid body rotation in convective zones.

It is possible to consider only the hydrostatic effects of rotation and/or to include also the internal angular momentum redistribution and surface angular momentum loss.

3.2. Atmospheric treatments

In addition to the gray atmospheric boundary conditions in the version by Mendes et al. (1999), the ATON2.4 code can now adopt non-gray atmospheric integration. In the first case the internal structure is matched at $\tau = 2/3$ with the values of P and T found via a Krishna-Swamy (1966) $T(\tau)$ relation. In the non-gray case we can choose the optical depth at which the matching is done: typical values are in the range $1 \leq \tau \leq 100$. For the atmospheric structure we can choose among several sets of models: (1) either the MLT or the FST models by Heiter et al. (2002); (2) the AH+AHS grid, based on the NextGen models by Allard & Hauschildt (1997), complemented by the low gravity models by Allard et al. (2000). To follow the evolutions starting from early, low-gravity stages we merged the NextGen tables (only available for $\log g \geq 3.5$) with the more recent low-gravity models ($2 \leq \log g \leq 3.5$). Eventually, we obtained rectangular tables in the range $2 \leq \log g \leq 6$ and 2000 K $\leq T_{\rm eff} \leq$ 6800 K.

[2] α is mapped in the domain $T_{\rm eff} = 4300$−7100 K, $\log g = 2.54$−4.74.

[3] The FST convection model corresponds to *very efficient convection*, as shown by the quasi-coincidence of the resulting tracks with the tracks employing the MLT α calibrated on the 2D hydrodynamic models. We find confusing and misleading the statement by Baraffe et al. (2002), who point out that the FST model is very *inefficient* in the upper solar layers, where it provides results that are not consistent with the hydrodynamic simulations of convection for the solar model (nevertheless, remember that the FST model provides a better fit than MLT for the spectrum of solar oscillations, see e.g. Canuto & Christensen-Dalsgaard 1998). What matters in the description of the pre-MS is the average efficiency of convection in the *whole* superadiabatic envelope, and this is very large for the FST, roughly corresponding to an α value in the MLT description somewhat larger than 2.

Table 1. Main physical parameters of the present models.

Parameter	Input
Mass	0.085–3.8 $M_\odot$
Boundary conditions	AH+AHS
Matching point	$\tau = 10$
Convection model	MLT
MLT parameter	$\alpha = 1.0$, 2.0 and 2.2
Rotation	Rigid body
Initial angular momentum	Kawaler (1987)
Opacities	IR93 and AF94
Equation of state	R96 and M88
Chemistry	$Y = 0.27$, $Z = 0.0175$
Initial X(D)	2×10^{-5}

3.3. Input micro-physics

The radiative opacities are taken from Iglesias & Rogers (IR93, 1993), extended by the Alexander & Ferguson (AF94, 1994) tables in the low-temperature regime. The OPAL equation of state (Rogers et al. 1996, R96) is used in the range $3.7 < \log T < 8.7$, while in the low-T high density regime we use the Mihalas et al. (M88, 1988) EOS. The nuclear network includes 14 elements and 22 reactions; the relevant cross-sections are taken from Caughlan & Fowler (1988).

3.4. Convection

The borders of the instability regions are found via the Schwarzschild criterion. The convective fluxes can be computed either by the FST model (Canuto et al. 1996), or by the MLT (Böhm-Vitense 1958); in the latter case the free parameter $\alpha = \Lambda/H_\mathrm{p}$ determining the mixing length can be arbitrarily selected.

4. Input of present models

We computed pre-MS stellar evolutionary tracks in the mass range $0.085 \leq M/M_\odot \leq 3.8$. We adopted the solar chemistry with $Z = 0.0175$ and $Y = 0.27$, while the starting deuterium abundance in mass fraction, following Linsky (1998), was set to $X(D) = 2 \times 10^{-5}$. The main physical parameters of the model sets are summarized in Table 1. The evolutions start from a fully convective configuration with central temperatures in the range $5.3 < \log T_\mathrm{c} < 5.8$, follows deuterium and lithium burning and ends at the main sequence configuration.

4.1. Boundary conditions

We compute gray models for comparison with previous results. For the non-gray models we use the AH+AHS grid. Following a suggestion by Heiter et al. (2002), we match the atmospheric grid with the interior integration at $\tau_\mathrm{ph} = 10$. This choice should minimize the consistency problems related to the different EOS and opacities adopted in the interior and in the atmosphere, and to the absence of turbulence pressure in the atmospheric modeling.

4.2. Choices about convection

As the FST atmospheric tables by Heiter et al. (2002) are available only for temperatures above $T_\mathrm{eff} = 4000$ K, they cannot be used to compute models below ~0.7 $M_\odot$ (Montalbán et al. 2004). In particular, they cannot be used to analyze the ONC stellar population, mainly concentrated at $T_\mathrm{eff} < 4000$ K. To achieve consistency between the internal and the atmospheric convective treatment, we decided to calculate only MLT models.

Apart from the quoted cases in which α can be calibrated on hydrodynamic models, the necessity to simplify the numerical treatment of convection leads stellar modelists to use a single α for the convection zone and for all the evolutionary phases. This choice is equivalent to adopting an average efficiency of the convective transport on the whole extension of the convective region, and on all the evolutionary phases. There is no good reason to assume that the α that, e.g., fits the solar radius should be used for other masses and for different evolutionary phases. Further, the efficiency of convection might change considerably within a convective zone, thus requiring the use of a variable α. Thus a preliminary investigation of the effects of changing this parameter is mandatory.

We computed sets of models with three different values of the parameter: the models with $\alpha_\mathrm{in} = 2.0$ (α2.0 set) allow a fit of the solar radius for non-rotating models[4]; the models with $\alpha_\mathrm{in} = 2.2$ (α2.2 set) are chosen to provide a "very efficient convection" set. Both these sets are termed HCE (high efficiency convection) sets. We further provide tracks with $\alpha_\mathrm{in} = 1.0$ (α1.0 set). This latter choice, according to D'Antona & Montalbán (2003, confirmed in Sect. 5.4), leads to a better agreement with the lithium vs. T_eff relation observed in young open clusters stars. Remember, however, that the adopted BCs come from model atmospheres computed, down to $\tau_\mathrm{ph} = 10$, with $\alpha_\mathrm{atm} = 1.0$. (see the discussion in Sect. 2.5 and in Montalbán et al. 2004). We show in Fig. 1[5] the comparison between tracks and isochrones of these three sets, showing the well known fact that both masses and ages are affected by the choice of the convection model.

4.3. Initial angular momentum

Rotation was modeled according to the rigid body law. This choice is motivated by the fact that most of the low mass stars are still fully convective in the evolutionary stages of interest for this study. As a first attempt, the initial angular momentum J_in for all models was estimated according to the prescriptions by Kawaler (1987). In that work, a relationship between angular momentum and stellar mass for stars earlier than F0 was derived using main-sequence (MS) stellar models and an estimate of the mean initial angular momentum-mass relation was made for stars of later spectral type. As masses larger than about 1.5 $M_\odot$ do not lose much angular momentum during their early evolutionary phases, it can be assumed that these stars reach the MS with the same angular momentum that they had at the beginning of their evolution. Kawaler (1987) is able to reproduce the observational relation at $M > 1.5\ M_\odot$ using his own models for radiative stars, he then extends the models to lower mass stars. For these, however, the observations do not provide a direct comparison with the initial angular momentum, as their rotation has been slowed down during the main sequence lifetime (but not significantly during the pre–MS, if we adopt the hypothesis of pre–MS disk locking in the same way as Bouvier et al. 1997). For the range 0.6–1.25 $M_\odot$, the initial angular momentum-mass relation can be easily obtained from the respective mass-radius and mass-moment of inertia relations from Kawaler (1987):

$$J_\mathrm{kaw} = 1.566 \times 10^{50} \left(\frac{M}{M_\odot}\right)^{0.985} \quad \mathrm{cgs}. \tag{1}$$

[4] Also Baraffe et al. (1998) and Montalbán et al. (2004) find a similar α_in (=1.9) to reproduce the solar radius.

[5] Figure 1 and all others that use theoretical results were made with rotating models.

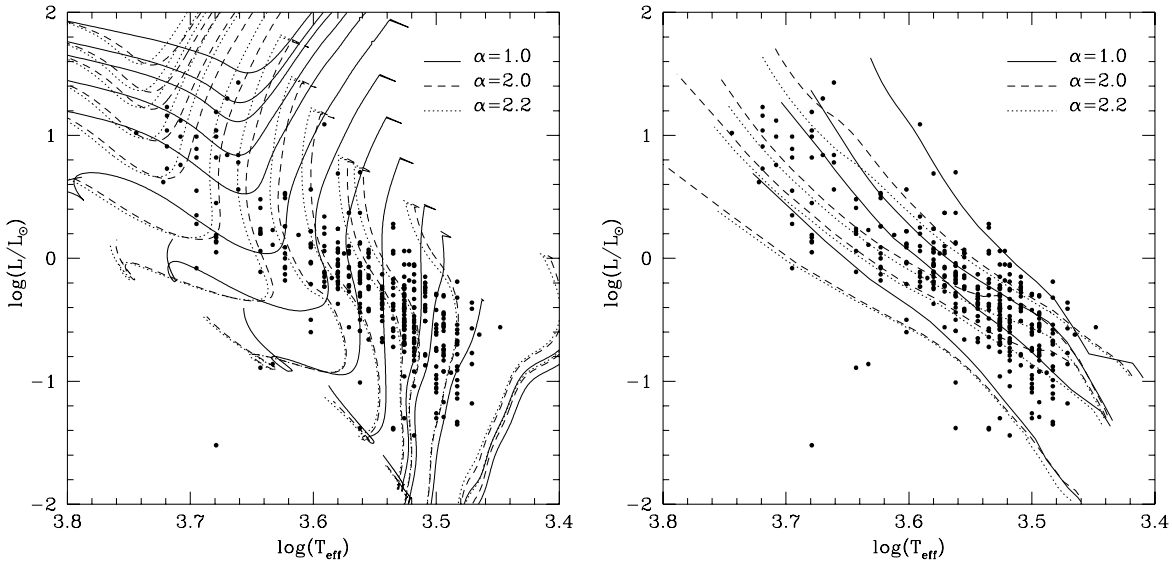

Fig. 1. Paths followed by the theoretical tracks (*left*) and isochrones (*right*) of the rotating models calculated with three different values of the free parameter α determining the mixing length. For clarity, we report only the following masses calculated with our three sets of tracks (α1.0, α2.0, α2.2): 0.09, 0.1, 0.2, 0.3, 0.35, 0.5, 0.7, 1.0, 1.4, 2.0, 2.5, 3.0, 3.3 and 3.8 $M_\odot$ from bottom to top. The observational data from Hillenbrand (1997) are represented by • symbols.

Once started with this initial angular momentum, we keep it constant in our models during the pre–MS according to the above mentioned hypothesis, whose validity will be checked later. This expression will then be extended to smaller masses as a result of the present study. The comparisons made in this work will help us to calibrate different models of angular momentum evolution.

5. First comparisons among models

5.1. The role of the D-burning

An uncertainty that deserves a separate discussion is the abundance originally assigned to deuterium. Deuterium burning, at least in the classic scenario, takes place in the early phases of the pre-MS evolution, when the central temperatures reach $T \sim 10^6$ K. A higher deuterium abundance does not alter the track location, but stretches the duration of the D-burning phase itself, thus determining a delay in the evolution. We calculated for comparison a set of tracks with double deuterium abundance, $X(D) \sim 4 \times 10^{-5}$, that is the highest value acceptable on observational grounds (Linsky 1998). In comparing the two sets of tracks, we note the following:

1. the track location does not change;
2. for $M > 0.5\,M_\odot$, the high-D evolutions are slower, but the age difference is in all cases shorter than 200 000 yr;
3. for $M < 0.4\,M_\odot$, the age differences between tracks of the same mass are no longer negligible, from ∼250 000 yr for $M = 0.4\,M_\odot$ to ∼600 000 yr for $M = 0.2\,M_\odot$.

In terms of the general conclusions found during the analysis of the ONC stellar population, increasing the D abundance would have no effect on the mass distribution, while the age distribution would be shifted to slightly older ages.

5.2. Role of non-grayness

The gray tracks of models with $\alpha = 1.0$ are systematically hotter than their non-gray counterparts, although the difference in $T_{\rm eff}$ varies with the mass. For the lowest masses of our sample, i.e. $M \leq 0.2\,M_\odot$, the high gravities allow the differences to remain within $\Delta T_{\rm eff} \sim 100$ K. This difference increases to ∼250 K at $0.6\,M_\odot$ and reaches a maximum of ∼400 K in $1\,M_\odot$ models only at the end of the Hayashi track. The stars for which the pre-MS tracks are most sensitive to the boundary conditions are those with masses in the range $0.4\,M_\odot \leq M \leq 1\,M_\odot$: the difference in $T_{\rm eff}$ slightly increases along each track, and reaches a maximum of $\Delta T_{\rm eff} \sim 400$ K when the radiative core is formed. The $T_{\rm eff}$ of more massive stars are less influenced by the atmospheric treatment. These differences in $T_{\rm eff}$ lead to the assignment of a different mass to a given observed star. We verify that, consistent with the above discussion, this effect is negligible for the lowest masses, while it leads to differences of the order of $\sim 0.1\,M_\odot$ for $M \sim 0.3$–$0.5\,M_\odot$, where, as we shall see, the bulk of the ONC population is found. For larger masses the differences are larger because the tracks for different masses are closer to each other.

5.3. The convection model

The tracks corresponding to the three values of α used in the present investigation are shown in the left panel of the Fig. 1. The observed stellar loci are also reported. In the early phases, with the exception of the D-burning phase, gravitational contraction is the only source of energy. The densities and temperatures increase until the central regions become radiatively stable; shortly after, H-burning takes over as the main energy source. We see from the left panel of the Fig. 1 that the α2.0 and α2.2 tracks are systematically hotter, the differences being larger for higher masses and smaller for older ages. This behavior can be understood on the basis of the different degree of overadiabaticity present in the various masses at different ages. The exact temperature profile depends on the overadiabaticity ($\nabla - \nabla_{\rm ad}$), which is defined as the excess of the effective temperature gradient in comparison with the adiabatic temperature gradient, and it is only noticeably different from zero at the border of the convective zone, where convection becomes inefficient. The two panels of Fig. 2 show, respectively, the evolution of the overadiabaticity at $\tau = 10$ and of the width (in solar masses) of the external region of the star where $(\nabla - \nabla_{\rm ad}) > 10^{-4}$. For clarity we report

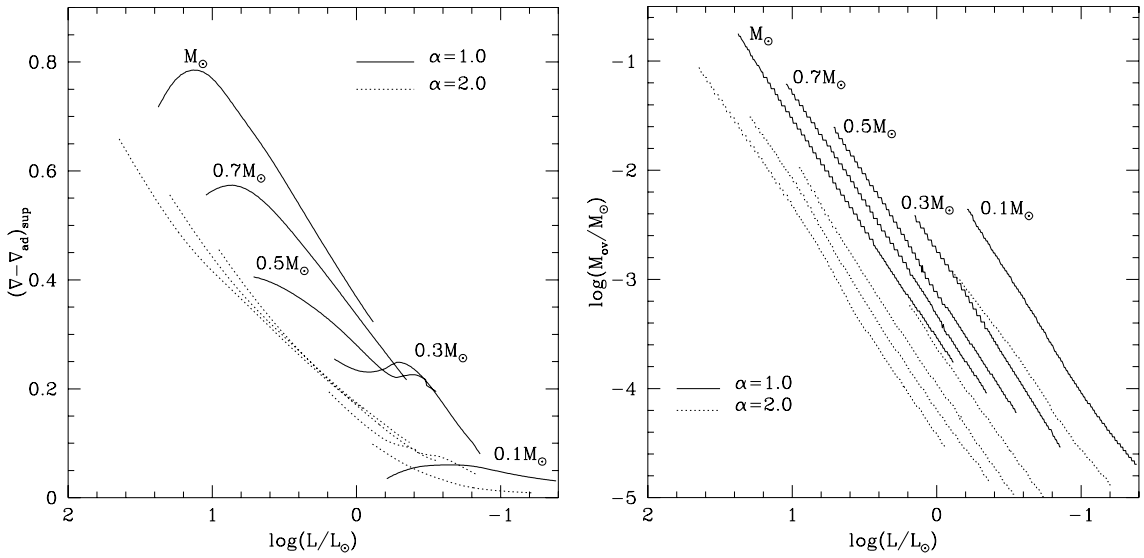

Fig. 2. *Left*: variation with luminosity of the overadiabaticity of the stellar layer at $\tau = 10$ of some pre-MS models calculated with different values of the parameter α entering the mixing length expression. *Right*: the variation with luminosity of the fraction of the mass of the star where $(\nabla - \nabla_{\rm ad}) > 10^{-4}$, for the same masses shown in the left panel. For clarity we show only models α1.0 and α2.0.

only the α1.0 and α2.0 models. The luminosity is on the abscissa as a time indicator. A detailed inspection of Fig. 2 shows:

1. the overadiabaticity at $\tau = 10$ of the α1.0 models is systematically higher than their α2.0 counterparts. This can be understood on the basis of the intrinsic lower efficiency of the convective model adopted, due to a lower mixing length;
2. due to the higher internal densities of the less massive models (hence, greater convective efficiencies), the overadiabaticity differences increase with the mass;
3. in the less massive models the differences above tend to narrow with age;
4. the extension in mass of the overadiabatic region is also systematically higher in the α1.0 models, and tends to shrink with age.

We verified that models of the same mass belonging to the two sets of tracks follow the same $L(t)$ relation. The differences in the location of the tracks are, therefore, to be totally ascribed to differences in the effective temperatures. Since the interior of these structures is practically adiabatic (in the center, $(\nabla - \nabla_{\rm ad}) < 10^{-7}$ in all cases), the radius is mainly determined by the degree of the overadiabaticity. This explains why larger differences are found for higher masses. In the lowest masses the efficiency of convection increases at older ages, so that the sensitivity to the adopted model for convection is strongly reduced. The low mass tracks approach each other at low luminosities (see Fig. 1).

5.4. The lithium depletion

Table 2 shows the lithium concentrations for our three sets of tracks and their non-rotating counterparts. We report the values for 0.7, 0.8, 0.9, 1.0 and 1.2 $M_\odot$ at 10^8 yr. A comparison between log N[Li] found with rotating and non-rotating models, keeping α fixed, is qualitatively in agreement with the abundances found by Mendes et al. (1999), i.e., rotating models provide greater lithium depletion especially for low-mass stars at the age in question. Another comparison between the abundances found with different values of α, keeping the rotation status fixed, confirms the results by D'Antona & Montalbán (2003): the lithium depletion of the HCE models is too large to be consistent with the lithium depletion observed by Soderblom et al. (1993) and Garcia Lopez et al. (1994) in young open clusters, which can be reproduced only by the LCE α1.0 models. On the contrary, the solar radius is reproduced only by the α2.0 model, and 2D hydrodynamic computations indicate HCE in the pre-MS. We regard this result as an indication that the efficiency of convection in the pre-MS might be affected by other parameter(s). The "second parameter" affecting lithium depletion is identified as the stellar rotation rate by Siess & Livio (1997) and in the papers by Ventura et al. (1998) and D'Antona et al. (2000). The first authors propose that α is smaller in fast rotating pre–MS stars due to the twisting of convective cells, the others show that the action of the dynamo-induced magnetic field due to the interaction of rotation and convection modifies the structure of the convective layers and reduces lithium depletion.

Table 2. Lithium abundances at the age of 10^8 yr for 0.7, 0.8, 0.9, 1.0 and 1.2 $M_\odot$. We report the values obtained with different sets of our non-gray models, with ("rot") and without ("non-rot") rotation. The initial lithium concentration is $\log N$[Li] = 3.31.

Models	0.7 $M_\odot$	0.8 $M_\odot$	0.9 $M_\odot$	1.0 $M_\odot$	1.2 $M_\odot$
rot α = 1.0	0.750	2.607	3.087	3.226	3.291
rot α = 2.0	−0.781	1.669	2.267	2.720	3.139
rot α = 2.2	−0.961	1.466	2.109	2.592	3.094
non-rot α = 1.0	0.950	2.650	3.097	3.228	3.291
non-rot α = 2.0	−0.524	1.715	2.295	2.733	3.143
non-rot α = 2.2	−0.521	1.712	2.297	2.733	3.143

6. Comparison with the ONC stars

6.1. Data from the literature

In order to study angular momentum evolution in pre-MS phase, we will compare our sets of evolutionary tracks with observational data of the ONC stars. To accomplish this goal we need some key parameters, such as effective temperatures and luminosities (to infer masses and ages of the stars) and also the rotation period and an index that allows us to distinguish between different kinds of angular momentum evolutions.

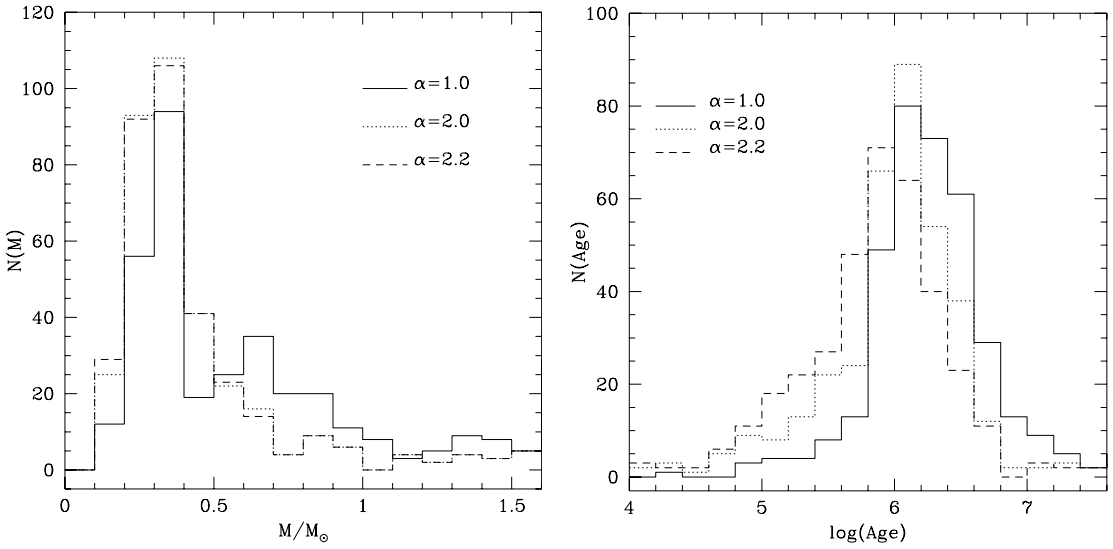

Fig. 3. Mass (*left*) and age (*right*) histogram based, respectively, on the masses and ages assigned to the observed stars in the ONC using three different sets of tracks, calculated with three prescriptions for convection, α = 1.0, 2.0 and 2.2.

The ONC data we used have been kindly provided by Dr. Keivan Stassun, who has widely worked on the rotational properties of ONC (Stassun et al. 1999, 2004). Our final study sample is composed of a combination of data from the following sources:

1. Rotation periods: Stassun et al. (1999), Herbst et al. (2002);
2. Effective temperatures and luminosity: Hillenbrand (1997);
3. Infrared continuum excess, $\Delta[I-K]$: Hillenbrand et al. (1998);
4. Ca II equivalent width, EW(Ca II): Hillenbrand (1997), Hillenbrand et al. (1998);
5. X-ray luminosities: Stassun et al. (2004).

The rotation period diagnostic was obtained by photometry, interpreting as rotation the periodic photometric variability, probably due to the presence of stellar spots.

The IR excess ($\Delta[I-K]$) was obtained from combined optical and infrared photometric data. Extinction and spectral typing uncertainties are the main sources of errors in $\Delta[I-K]$ estimates. For earlier spectral type stars ($\lesssim$K2) the errors are negligible (<0.05 mag), for spectral types in the range K2−M3, typical errors are between 0.1−0.3 mag, and it is largest for the latest spectral types, where mis-classification causes relatively larger errors.

The EW(Ca II) was obtained from the optical spectroscopic study of Hillenbrand (1997) and analyzed by Hillenbrand et al. (1998). Their measurements uncertainty is estimated at 0.5 Å based on measurements of multiple spectra of the same star.

In order to obtain more reliable values for L_X of ONC stars, Stassun (2004) reanalyzed all archival *Chandra*/ACIS observations of these objects using updated calibrations and including time-filtering of flares.

The effective temperatures and luminosities were obtained from optical spectroscopy and photometry.

6.2. Derivation of masses and ages

For each of the three sets of tracks previously discussed, we assigned to each observed point a mass and an age by linearly interpolating between the two nearest tracks. An inspection of Fig. 1 can help understand, at least qualitatively, the differences that we should find by varying α. For each observed star in the α2.0 and α2.2 sets, we assign a systematically smaller mass than in the α1.0 models, hence a younger age (we recall that this evolutionary phase is governed by gravitational contraction, that proceeds on a Kelvin-Helmoltz time scale $\tau_{\rm KH} \propto \frac{M^2}{RL}$). If the α2.0 or α2.2 sets are used, we therefore expect a mass distribution shifted to lower masses and, on the average, a younger population. Typical internal errors are $\lesssim$0.2 dex in $\log(L/L_\odot)$ for all spectral types and are $\lesssim$0.02 dex in $\log T_{\rm eff}$ for late-type (K−M) stars, but increase towards earlier spectral types. This leads to an uncertainty in the determination of mass that is $\lesssim$0.1 $M_\odot$ for $M < 0.5\ M_\odot$, and gradually increases to $\sim$0.2 $M_\odot$ for $M \sim 1\ M_\odot$. The attribution of age is mainly influenced by the uncertainty on the luminosity, that makes the age uncertain by $\sim$1 Myr at the age of 1 Myr. This poses the problem of whether the age distribution we find should be considered either as the result of a burst of star formation or as a real indication of age differences from star to star. In the course of the investigation we favour a statistical interpretation of data as an indication of some age evolution, based on the evolution of rotation periods.

The left panel of the Fig. 3 shows the mass distribution of the observed stars, obtained by using the three sets. Only masses $M < 1.6\ M_\odot$ are plotted because they represent most of the stars in the sample. The mass function for the α1.0 set peaks in the mass interval 0.3−0.4 $M_\odot$, but we also note the presence of a significant group of stars with masses in the range 0.2−0.3 $M_\odot$ and another group in the interval of 0.6−0.9 $M_\odot$. For the HCE models this latter group of objects becomes less relevant and the mass function peaks in the mass interval 0.2−0.4 $M_\odot$. The right panel of Fig. 3 confirms that the age distribution depends on the choice of α. We note that a slightly younger population is obtained as the value of α increases, and, in the α2.0 and α2.2 cases, a very young group of stars appears at ages $\sim 1-2 \times 10^5$ yr, but is not present for the LCE (α1.0) models. This can be understood by considering, in the right panel of Fig. 1, the relative location of observed points and theoretical isochrones. The age differences are also due to the different slope of the isochrones corresponding to the two sets of tracks, which, in turn, are related to the differential variation of temperature with mass, already outlined in Sect. 5.3. In the HCE models there is a group of objects with ages clustering around 100 000 yr . For the α2.0 case this young

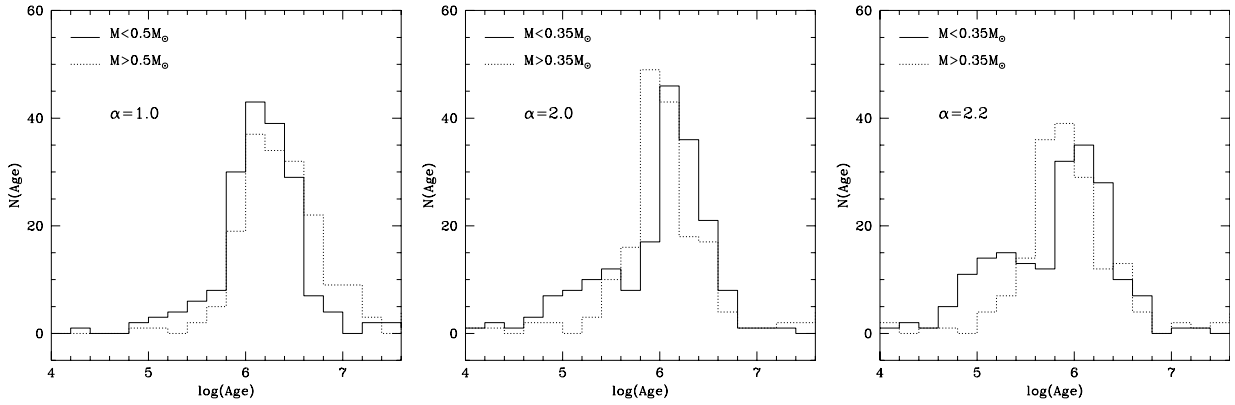

Fig. 4. The comparison between the age distributions of the observed stars with assigned mass lower and higher than $M_{\rm tr}$. The $M_{\rm tr}$ value is 0.5 $M_\odot$ for LCE models and 0.35 $M_\odot$ for HCE models.

group is made up of ∼40 stars and for the α2.2 set its presence is still more evident, exhibiting ∼70 objects.

In Sect. 7.1 we will define a transition mass $M_{\rm tr}$ for HCE and LCE models, on the basis of the rotational periods distribution. Here we compare, in Fig. 4, the age distribution for two different ranges of mass, $M > M_{\rm tr}$ and $M < M_{\rm tr}$. We see from the left panel of Fig. 4 that in the α1.0 set the two populations show a similar distribution. On the contrary, the age distribution of the two groups for HCE models is very different. Thus, while the existence of a group of younger stars would be possible in the formation history of the ONC, it should be present for any mass. The discrepancy in the age distribution may be again an indication that the α1.0 set provides a better description of the ONC stellar population, in agreement with the lithium depletion discussed in Sect. 5.4 and with the previous analysis made by D'Antona & Montalbán (2003). In any case, this certainly is not final and we proceed with the analysis by using the three sets of tracks.

6.3. Comparison with gray models

We compare now the effects introduced by the two major factors, i.e. convection and boundary conditions. Although for masses $M > 1\ M_\odot$ the treatment of convection is more relevant than the boundary conditions adopted in determining the effective temperature of the tracks (Montalbán et al. 2004), for the interesting range of mass for the ONC comparison, namely 0.2–0.4 $M_\odot$, and the non-gray models, convection is important mainly in the early evolutionary phases. At later phases (ages >1 Myr), convection becomes more adiabatic and the non-grayness becomes the main factor affecting the track location.

For gray atmospheric treatment, keeping α fixed to 1.0 would concentrate the same mass distribution at $M \sim 0.2$–$0.3\,M_\odot$. There would also be a considerable reduction of the population with masses in the range $0.6 < M/M_\odot < 1$. A larger effect would be obtained if we had used gray models with $\alpha = 2.0$. In this case, the mass function would be peaked in the range $0.1 < M/M_\odot < 0.3$, and the average age of the observed stars would be slightly younger than ∼1 Myr. This latter result was obtained by Herbst et al. (2002) during their analysis of the ONC population using the tracks by D'Antona & Mazzitelli (1994) that use gray approximation and the very efficient FST model for convection.

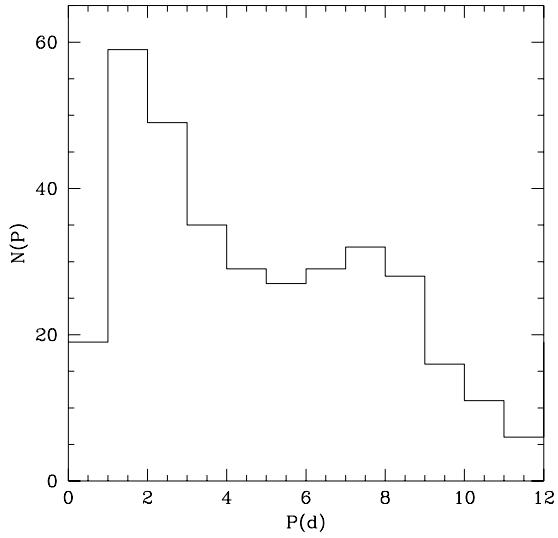

Fig. 5. The period histogram of all observed ONC objects. The total distribution of periods has a bimodal character, showing a primary peak of fast rotators ($P \sim 2$ days) and a secondary peak of slow rotators ($P \sim 8$ days).

7. Stellar rotation in the ONC

7.1. The dichotomy in period distribution for different mass ranges

We examine in Fig. 5 the distribution of the observed rotation periods. We note the presence of a primary peak corresponding to fast rotators with $1 \lesssim P(\mathrm{d}) \lesssim 3$, and a secondary peak at $P \sim 8$ d. The former can be associated with spin up due to the conservation of the total angular momentum. The latter indicates the presence of a mechanism acting to prevent stellar spinning up, at least in the early evolutionary phases. Attridge & Herbst (1992), Choi & Herbst (1996) suggested that this can be due to a "disk locking", due to magnetic coupling between the star and the disk (Königl 1991). Following Herbst et al. (2002) we investigate in detail the rotational status of the various masses involved. The rotational properties of the stars vary considerably with mass: stars with masses larger than a value $M_{\rm tr}$ have a clearly bimodal distribution, while the less massive sample contains only a tail of slow rotators. This behavior was first observed by Attridge & Herbst (1992) and discussed by Herbst et al. (2002). We define the "transition mass" ($M_{\rm tr}$), which depends on the track set chosen for the analysis, in order to maximize the effect of the

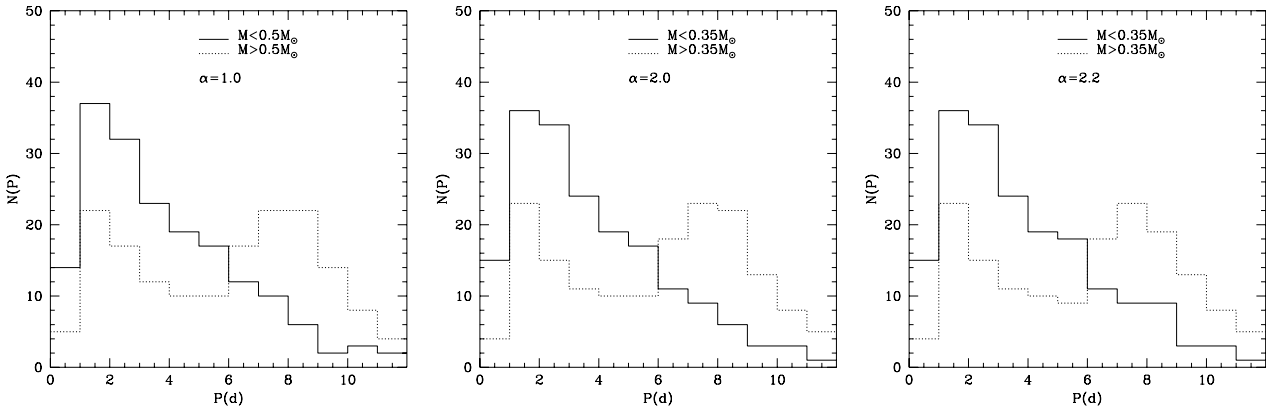

Fig. 6. Period histograms showing the dependence on mass of the period distribution of the ONC objects. Stars more massive than $M_{\rm tr}$ have a bimodal period distribution and their less massive counterparts rotate faster and exhibit a unimodal distribution. This behavior can be seen independently of the choice of α. The $M_{\rm tr}$ value is the same used in Fig. 4.

Table 3. Main physical parameters of the present gray (G) and non-gray (NG) models. $\mathcal{N}_<$ ($\mathcal{N}_>$) is the percentage of the $N_{\rm t}$ stars that have mass less (greater) than $M_{\rm tr}$ for different rotation periods (P). See text for details.

Models	Mass range ($M_\odot$)	Age range (Myr)	$M_{\rm tr}$ ($M_\odot$)	$\mathcal{N}_<$ $P<4$ d	$\mathcal{N}_<$ $P>6$ d	$\mathcal{N}_>$ $P>6$ d
G $\alpha=1.0$	0.2–0.3	0.6–2.5	0.35	65%	19%	53%
G $\alpha=1.5$	0.1–0.3	0.3–1.3	0.25	65%	19%	54%
NG $\alpha=1.0$	0.2–0.4	1–2	0.5	63%	18%	53%
NG $\alpha=2.0$	0.2–0.4	0.6–2.5	0.35	67%	18%	55%
NG $\alpha=2.2$	0.2–0.4	0.4–1.6	0.35	67%	23%	54%

bimodality. Although the dichotomy does not depend on the chosen set, the transition mass varies according to it. For LCE models it is 0.5 $M_\odot$, while a reasonable value is 0.35 $M_\odot$ for HCE models. If we had used our gray models with $\alpha = 1.5$, $M_{\rm tr}$ would have been still smaller, namely, 0.25 $M_\odot$, in agreement with the findings by Herbst et al. (2002), who used the HCE FST models by D'Antona & Mazzitelli (1994). In Fig. 6 we show the histogram of periods, respectively, for stars less and more massive than $M_{\rm tr}$. The secondary peak at $P \sim 8$ d, already seen in the Fig. 5, is present only in the population at $M > M_{\rm tr}$, while the low mass objects show a clear trend towards short periods. Table 3 shows the percentages of slow and fast rotators (here defined by the limitations $P > 6$ d and $P < 4$ d). Fast rotators contains more than 60% of masses $<M_{\rm tr}$. On average, only 20% of the masses $<M_{\rm tr}$ and ~54% of the masses $>M_{\rm tr}$ have $P > 6$ d.

This dichotomy indicates that either (i) disk locking is responsible for the presence of the secondary peak, and stars with $M > M_{\rm tr}$ tend to be embedded in their disk longer than their low mass counterparts, (ii) the locking time is similar, but the masses $>M_{\rm tr}$ evolve faster and a larger fraction of their pre–MS lifetime is locked, or (iii) the "locking period" of the group with $M < M_{\rm tr}$ is significantly lower than ~8 d. Our analysis confirms possible interpretations of the observed distribution of periods given by Herbst et al. (2002) (see their Fig. 15). The uncertainty on the convection model simply alters the transition mass from ~0.25 $M_\odot$ to a maximum of 0.5 $M_\odot$ for LCE models.

7.2. Disk locking and the disk lifetime

Following the suggestion by Herbst et al. (2002), that the longer period peak in the distribution indicates that some stars are locked in their disks with a period near 8 days, we simply considered the stars with periods larger than a threshold period ($P_{\rm thresh}$), which we put at 8d, as locked. For stars at $P < P_{\rm thresh}$, unlocked stars according to our criterion, we determine the epoch at which their period was equal to 8 days. This would be the time at which the stars would have lost their disks, and began a constant angular momentum evolution. Here we consider that angular momentum losses by magnetic braking are negligible at the pre–MS, since its timescale is much longer than the evolutionary timescale during pre–MS evolution. The temporal variations of radius and angular velocity were determined on the basis of our tracks once the mass was assigned. Following this hypothesis, we found some stars which had $P = P_{\rm thresh}$ at an age younger than 10^5 yr. In our interpretation, these stars have lost their disks very early and can be considered to have evolved without a disk. In this way, we identify three distinct populations:

1. early fast rotators – stars locked only for ages $<10^5$ yr;
2. slow rotators – stars probably still disk embedded;
3. moderate rotators.

Stars in the last group may have lost their disks at ages greater than 10^5 yr. They represent, on average, ~45% of the stars of the whole sample and this percentage do not change significantly with the choice of α. As long as the assumption that the locking period is independent of mass is valid, the disks seem to survive longer for higher masses. For all sets of tracks, the percentage of early fast rotators is ~40% for $M < 0.4\ M_\odot$, and gradually drops below ~12% for $M > 0.6\ M_\odot$.

The mass distribution of the slow and early fast rotators is shown in Fig. 7. We note, in particular, the maximum at 0.6–0.8 $M_\odot$ (for LCE models) and 0.3–0.5 $M_\odot$ (for HCE models) characterizing the slow rotator population (dotted line). We can compare the fraction of early fast rotators identified in the ONC with the non-accreting fraction of TT and Brown Dwarfs in star forming regions of similar ages (ρ Oph and Taurus, Mohanty et al. 2005). The lower limit to this non-accreting fraction is ~35%, not very different from our result.

In our analysis we use the rotation period as an indicator of the presence of a disk surrounding these stars. In order to test the reliability of this hypothesis, we should use several observational indicators of the presence of disk and accretion, like the infrared excess $\Delta[I-K]$, the equivalent width of Ca II line, the excess in the L-band and H_α, Ca, O emission lines. Near IR excess as disk indicators and EW Ca II as accretion diagnostic must be used with caution (Hillenbrand 1997). But, as this is mainly a theoretical work, we will check what is already in the literature

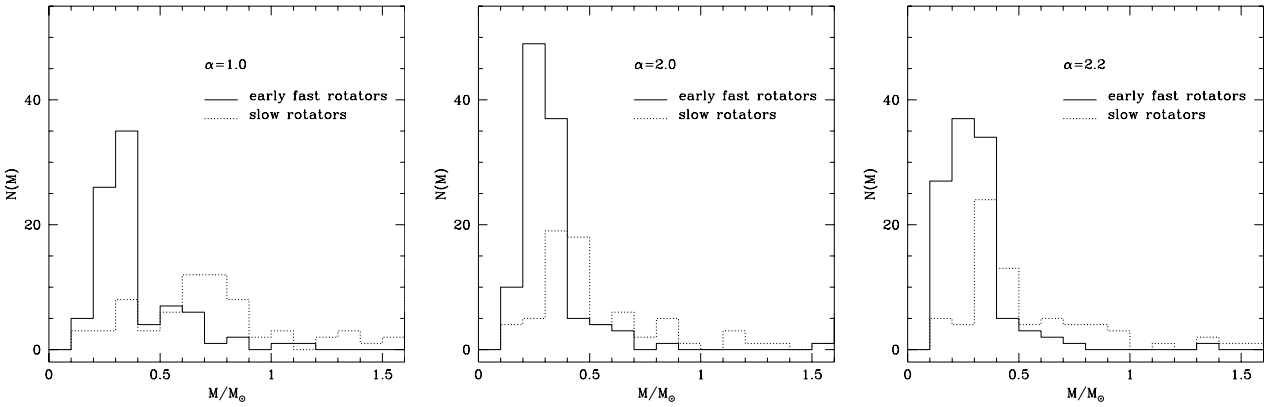

Fig. 7. The mass distribution of the sources which according to our analysis rotate fast since early evolutionary phases (solid lines) compared to those that are slow rotators in the current epoch (dotted lines). This comparison is shown for the three sets of models (α1.0, α2.0 and α2.2).

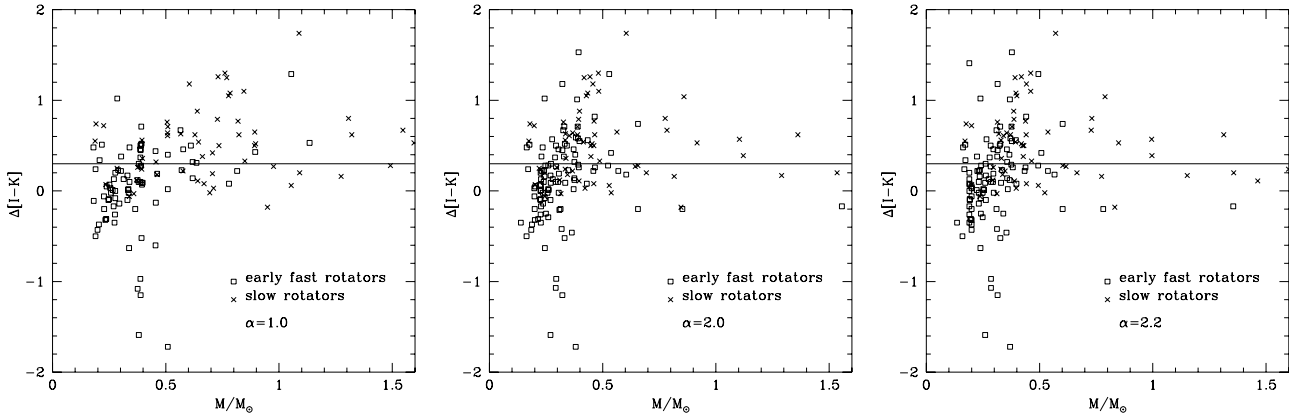

Fig. 8. The observed infrared excess of our sample stars plotted against their inferred mass according to the three sets of models used in this work.

for ONC stars, namely IR excess $\Delta[I-K]$ and *EW* Ca II, mainly as additional arguments.

It is expected that still locked stars have $\Delta[I-K] > 0.3$, and those that evolved without disk should have infrared excess significantly lower than this threshold value (Herbst et al. 2002). We report in Fig. 8 the observed stars on the plane $\Delta[I-K]$ vs. mass. We can see that sources that we identified as still locked (slow rotators – crosses) are mainly concentrated above the $\Delta[I-K] = 0.3$ line, while those that evolved without a disk (early fast rotators – open squares) lie mainly below it, for the three sets of models. This straight correlation between the infrared excess and our derivation of the presence of a disk agrees with our theoretical considerations.

The equivalent width of Ca II lines is commonly used as an indicator of an active accretion process. For accreting stars we expect emission lines and $EW(\mathrm{Ca\,II}) < -1$, while for non-accreting objects we have $EW(\mathrm{Ca\,II}) > 1$ (Flaccomio et al. 2003b). We cannot expect a direct correlation between $\Delta[I-K]$ and $EW(\mathrm{Ca\,I})$, because some stars might still have a disk, although no longer accreting. Yet, we expect that the observed stars with $EW(\mathrm{Ca\,II}) < -1$ and $\Delta[I-K] > 0.3$ should have a disk surrounding them, and the disk locking mechanism should be active. We could identify ∼40 stars with known rotational periods that satisfy both requests, about 30% of which are actually identified as still disk embedded according to our criterion ($P > P_{\mathrm{thresh}} = 8$ d). Part of the remaining have long rotational periods, very close to P_{thresh}, which suggest the presence of a disk.

7.3. An alternative view: the role of the magnetic field

The idea that disk-locking is responsible for the dichotomy observed, which eventually leads to the presence of two peaks in the distribution of periods of the ONC stars, was recently criticized by Barnes (2003), who argued that the possible role of disks can be only to set an initial distribution of periods, since disk-locking should affect all the stars equally.

Based on the observed color-period diagrams of several open clusters (e.g. IC 2391, α Per, Pleiades, M 34, etc.), Barnes (2003) found that a double population with distinct rotational properties characterizes any stellar association. Further, he found that a systematic trend with age is apparent, namely that older clusters have a smaller number of rapid rotators, that eventually disappear at ages ∼800 Myr.

Barnes (2003) interpreted these observations as a result of a different morphology of the magnetic field configuration. According to his suggestion, rapid rotators have small scale magnetic fields associated with their convective region, which cannot be anchored either to the inner radiative core or to the star's external layers. All the fully convective stars should belong to this group. Conversely, the slowly rotating stars are characterized by large scale magnetic fields, probably associated with the presence of an interface dynamo between the external convective region and the internal radiative zone. In this case the process of spinning down the star is much more efficient. The dynamo, that is probably created by the decoupling between the convective and radiative zones, anchors the spun-down convective envelope to the rapidly rotating core, thus favouring a constant migration

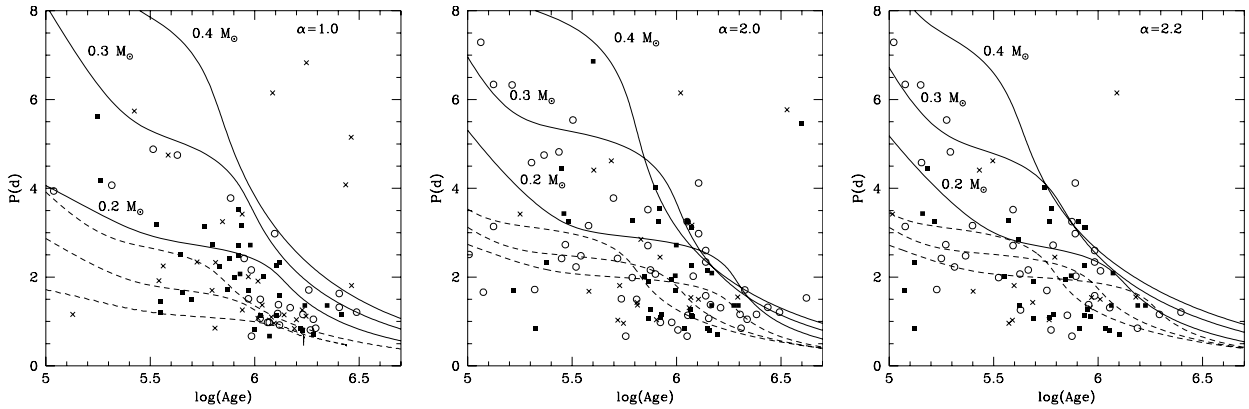

Fig. 9. The temporal evolution of the periods of our three sets of models with mass in the range $0.2\,M_\odot \leq M \leq 0.4\,M_\odot$ evolved starting with an initial angular momentum calculated on the basis of the Kawaler (1987) prescription (solid lines), and with the same values multiplied by a factor of 3 (dashed lines). The stars that we suppose to be evolved with a constant angular momentum, i.e., without a disk, are also shown. The ∘ symbols identify the mass range $0.2 < M/M_\odot < 0.3$, ■ is used for $0.3 < M/M_\odot < 0.4$, and × for all the other masses.

of the stars belonging to the rapidly rotating group to the slowly rotating sample. This should explain the complete absence of the fast rotator sequence at old ages (see Barnes 2003, Fig. 1). Due to the young age of the ONC, both populations should be present there, as we find. This interpretation is not correct if we take our results at face value: if we rely on our attribution of masses and ages, the great majority of the stars observed are indeed fully convective, i.e. should all belong to the rapidly rotating sequence. We suggest that the magnetic field itself plays a role in inhibiting convection (Gough & Tayler 1966; Moss 1968; Ventura et al. 1998) and favours an earlier appearance of a radiative core in the stars having $M > M_{\rm tr}$. Consequently, we do not reject the idea that the presence of a double population is indeed due to the magnetic field configuration, rather than to the effects of a disk-locking mechanism.

7.4. A constant angular momentum evolution?

For those stars that we identified to have lost the disk in their early evolutionary phases, i.e., the early fast rotators, we may test the hypothesis that they evolved at constant angular momentum from the beginning. The distribution of these objects in the P vs. inferred age plane is shown in Fig. 9 for $\alpha = 1.0$, $\alpha = 2.0$ and $\alpha = 2.2$ models. We used different symbols as mass identifiers. We can see a clear trend towards shorter periods for older ages, especially for the $\alpha 1.0$ models, possibly indicating angular momentum conservation. We checked the possibility of reproducing the observed rotational pattern with age by means of our rotating models. This approach allows us to find out the range of initial angular momenta that, for each mass, must be used to calculate the models. We limit this analysis to the subsample of the mass range given in Table 3. We divided the observed sources into three classes of mass, indicated in Fig. 9 with open circles masses in the interval $0.2 < M/M_\odot < 0.3$, with full squares $0.3 < M/M_\odot < 0.4$ and with crosses all the remaining. The solid lines indicate the temporal variation of the rotational periods according to the evolution of our three sets of models with masses $M = 0.2, 0.3, 0.4\,M_\odot$ calculated by assuming an initial angular momentum following the prescriptions given in Eq. (1). We note that the temporal evolution of the periods vary with the parameter α, as it affects the radius of the stars. These curves can only reproduce the upper envelope of the observed loci, but, particularly at the ages shared by the bulk of the ONC stellar population, they lead to rotational velocities too slow with respect to most of the observed values.

To reproduce the rotation period of the fastest stars, we need to use an initial angular momentum at least three times larger than that prescribed by Kawaler (1987), if we use LCE models, and even larger for HCE models. To fully bracket the observed periods it is necessary to assume a distribution of initial angular momenta $J_{\rm in}$, at least, in the range $J_{\rm kaw} < J_{\rm in} < 3J_{\rm kaw}$. This result can be used to extend the Kawaler (1987) prescription to the very low mass stars.

7.5. The X-ray emission of the ONC stars

Flaccomio et al. (2003a, 2003b) and Stassun et al. (2004) performed deep analyses of the archival *Chandra* data and derived the $L_{\rm X}$ luminosity of all the sources included in the Hillenbrand (1997) sample. Their goal was to correlate $L_{\rm X}$ of pre-MS stars with the factors most likely driving the X-ray emission itself, i.e., accretion and rotation. Their main finding was the lack of a clear correlation between $L_{\rm X}$ and rotational period. They interpreted this result as evidence that the ONC pre-MS stars are indeed in the "super-saturated" regime of the rotation-activity relationship. This seems to be confirmed by the average value of the fractional X-ray luminosity $\log(L_{\rm X}/L_{\rm bol}) \sim -3.6$, that is slightly smaller than the main sequence saturation value of $\log(L_{\rm X}/L_{\rm bol}) \sim -3$.

Concerning the relationship between accretion and X-ray emission, Stassun et al. (2004) found that accreting stars have X-ray luminosities on average lower than their non-accreting counterparts, as a possible result of X-ray extinction by circumstellar gas in magnetospheric accretion columns. We could not find any clear correlation between EW(Ca II) and $L_{\rm X}$, although this might be a consequence of the smaller sample of stars with evidence of accretion (i.e. $EW(\mathrm{Ca\,II}) < -1$) used in the present work, compared to the complete sample by Hillenbrand (1997) and Hillenbrand et al. (1998) analyzed by Stassun et al. (2004).

We used our determinations of mass to look for any relationship between stellar mass and X-ray luminosity. In agreement with Flaccomio et al. (2003a), we find that $L_{\rm X}$ is correlated with mass (upper panels of Fig. 10). This trend is not due to a qualitative difference in the X-ray emissions, but rather to a general correlation between mass and bolometric luminosity (lower panels of Fig. 10). This is confirmed in Fig. 11, where we see that the $L_{\rm X}/L_{\rm bol}$ ratio is practically independent of mass for the three α models we have used. We note the high dispersion around

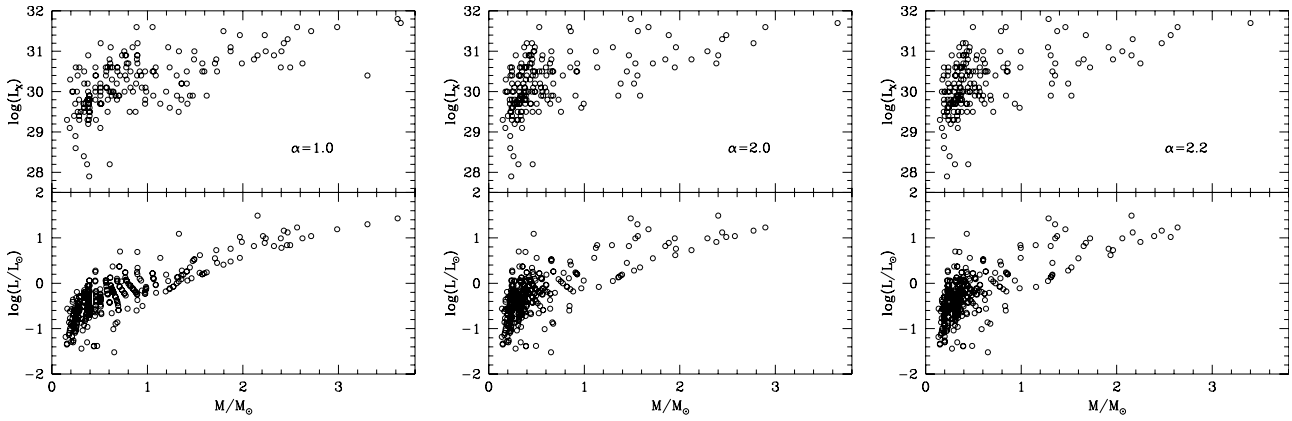

Fig. 10. *Top*: L_X luminosity (ergs/s) plotted against mass (obtained with our three sets of models) for the ONC observed sources with known rotational periods. *Bottom*: the same as top, with bolometric luminosity on the vertical axis.

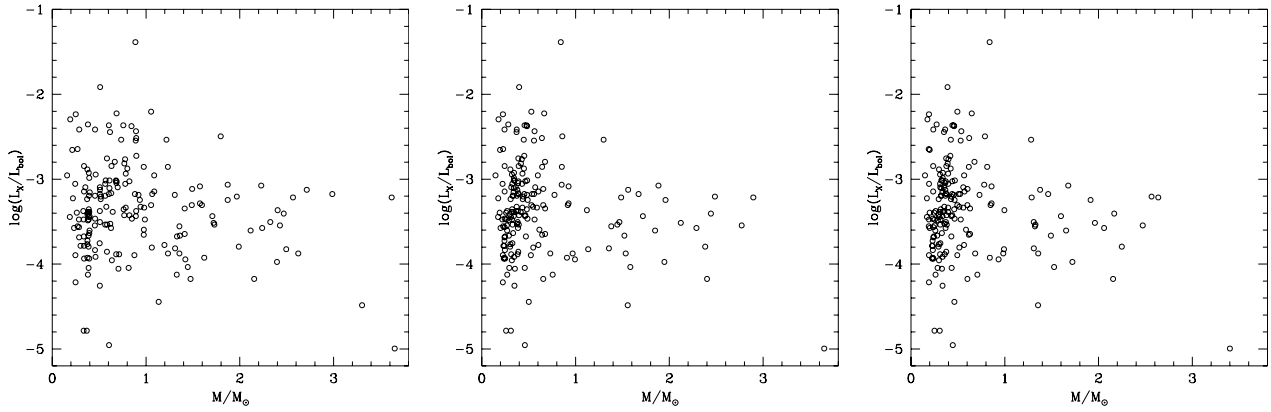

Fig. 11. The fractional X-ray luminosity as a function of mass for the same stars and models shown in Fig. 10.

the average value of $\log(L_X/L_{bol}) \sim -3.6$, present at the lowest masses, that is probably connected to the lower luminosities of these objects.

8. Conclusions

We use the observed stellar population of the ONC to test our pre-MS evolutionary tracks, to better understand the main physical properties characterizing the evolution of young stars. By comparing the location of the tracks in the HR diagram with the position of the observed objects, we assign to any single star a mass and an age, for three different convection efficient models.

We find the well known result that the treatment of convection is generally the most relevant physical input in determining the T_{eff} of pre-MS tracks in the HR diagram. The boundary conditions adopted also play a non-negligible role in determining the path followed by the evolutionary sequences on the HR plane. Gray models are systematically hotter than their non-gray counterparts. This effect, for the range of masses and ages at which most of the ONC population is found, has a similar quantitative effect as a change of the convective model. The use of non-gray models is recommended to describe these early evolutionary phases.

On the observational side, we find that the bulk of the observed stars in the ONC have masses in the range $0.2\,M_\odot \leq M \leq 0.4\,M_\odot$, for all non-gray models. The age distributions are more affected by the choice of the MLT parameter α. Ages are 1−2 Myr from the α1.0 set, 0.6−2.5 Myr for α2.0 set and 0.4−1.6 Myr for α2.2 models. This study confirms the presence of a dichotomy in the rotational properties between the objects with $M < M_{tr}$, whose period distribution peaks at short values, and stars with $M > M_{tr}$, that present a secondary peak at $P \sim 8$ d. The transition value of mass between the two populations is at $M \sim 0.5\,M_\odot$ for LCE and at $M \sim 0.35\,M_\odot$ for HCE models. If disk-locking is responsible for the secondary peak observed in the overall period distribution, these results can be interpreted by assuming either that the masses $M < M_{tr}$ lose their disk earlier, or that their locking period is shorter. The X-ray emission shows no correlation with period, supporting the suggestion that these stars are indeed in the super-saturated regime of the rotation-X ray luminosity relationship. The correlation of the X-ray flux with mass appears to be the consequence of the increased average luminosity of more massive objects.

For the low-mass stars that presumably evolved without a disk, we find that our results are consistent with an evolution-conserving angular momentum. The comparison between the model period evolution and the observed values suggests that initial angular momenta at least 3 times larger than those found by means of the Kawaler (1987) law are needed for stars with mass in the range $0.2\,M_\odot \leq M \leq 0.4\,M_\odot$. This analysis was not possible for the higher masses sample, due to the lack of a statistically meaningful sample of rapidly rotating stars.

The idea that the double population of the ONC can be explained on the basis of a different morphology of the stellar magnetic fields seems to be ruled out by the fact that almost all the observed sources are fully convective, according to our interpretation. However, a mechanism (e.g. the magnetic field itself) inhibiting convection might favour an earlier appearance of the

radiative core, at least in some of the stars. In our analysis we found other indications that convection in the pre-MS may be affected by other parameter(s): although 2D hydrodynamic simulations predict HCE in the pre-MS, we find two results in favour of LCE: (1) the lithium depletion in HCE models is too large to be consistent with the pre-MS depletion shown in young open clusters; (2) the age distribution derived from HCE models for two groups of smaller and higher masses is very different. It may be that the lower convection efficiency needed in the pre-MS is due to the structural effect of the dynamo-induced magnetic field, as suggested by Ventura et al. (1998) and D'Antona et al. (2000). This possibility leads us not to dismiss the idea of an earlier appearance of a radiative core in the $M > M_{\rm tr}$ group.

The evolutionary tracks (from 0.085 to 1.6 $M_{\odot}$) and isochrones (from 2×10^5 to 1×10^7 Myr) are available from the following web site: `www.mporzio.astro.it/~tsa`.

Acknowledgements. The authors thank Dr. Keivan Stassun for providing the observational data of ONC. Natália R. Landin would like to thank the Osservatorio Astronomico di Roma for their gracious hospitality during an extended visit. NRL and LPRV gratefully acknowledge financial support from the Brazilian agencies CAPES, CNPq and FAPEMIG.

References

Alexander, D. R., & Ferguson, J. W. 1994, ApJ, 437, 879 (AF94)
Allard, F., & Hauschildt, P. 1997, Nextgen, `http://dilbert.physat.uga.edu/~yeti/mdwarfs.html` (AH)
Allard, F., Hauschildt, P. H., & Schweitzer, A. 2000, ApJ, 539, 366 (AHS)
Asplund, M., Ludwig, H.-G., Nordlund, Å., & Stein, R. F. 2000, A&A, 359, 669
Attridge, J. M., & Herbst, W. 1992, ApJ, 398, 61
Baraffe, I., Chabrier, G., Allard, F., & Hauschildt, P. H. 1998, A&A, 337, 403
Baraffe, I., Chabrier, G., Allard, F., & Hauschildt, P. H. 2002, A&A, 382, 563
Barnes, S. A. 2003, ApJ, 586, 464
Basri, G., & Bertout, C. 1989, ApJ, 341, 340
Böhm-Vitense, E. 1958, Z. Astroph., 46, 108
Bouvier, J., Cabrit, S., Fernandez, M., Martin, E. L., & Matthews, J. M. 1993, A&A, 272, 176
Bouvier, J., Forestini, M., & Allain, S. 1997, A&A, 326, 1023
Canuto, V. M., & Christensen-Dalsgaard, J. 1998, Ann. Rev. Fluid Mech., 30, 167
Canuto, V. M., Goldman, I., & Mazzitelli, I. 1996, ApJ, 473, 570
Caughlan, G. R., & Fowler, W. A. 1988, Atomic Data Nucl. Tab., 40, 283
Chabrier, G., & Baraffe, I. 1997, A&A, 327, 1039
Choi, P. I., & Herbst, W. 1996, AJ, 111, 283
D'Antona, F. 1993, Inside the stars, Proc. of the 137th IAU Colloq., ed. A. Baglin, & W. Weiss, ASP Conf. Ser., 40, 395, San Francisco
D'Antona, F., & Mazzitelli, I. 1994, ApJS, 90, 467
D'Antona, F., & Mazzitelli, I. 1997, MmSAI, 68, 807
D'Antona, F., Ventura, P., & Mazzitelli, I. 2000, ApJ, 543, 77
D'Antona, F., & Montalbán, J. 2003, A&A, 412, 213
Endal, A. S., & Sofia, S. 1976, ApJ, 210, 184
Flaccomio, E., Damiani, F., Micela, G., et al. 2003a, ApJ, 582, 382
Flaccomio, E., Damiani, F., Micela, G., et al. 2003b, ApJ, 582, 398
Garcia Lopez, R. J., Rebolo, R., & Martin, E. L. 1994, A&A, 282, 518
Gough, D. O., & Tayler, R. J. 1966, MNRAS, 133, 85
Hartmann, L., Cassen, P., & Kenyon, S. J. 1997, ApJ, 475, 770
Hayashi, C. 1961, PASJ, 13, 450
Heiter, U., Kupka, F., van't Veer-Menneret, C., et al. 2002, A&A, 392, 619
Henyey, L. G., Lelevier, R., & Levee, R. D. 1955, PASP, 67, 154
Herbst, W., Bailer-Jones, C. A. L., Mundt, R., Meisenheimer, K., & Wackermann, R. 2002, A&A, 396, 513
Hillenbrand, L. A. 1997, AJ, 113, 1733
Hillenbrand, L. A., Strom, S. E., Calvet, N., et al. 1998, AJ, 116, 1816
Iglesias, C. A., & Rogers, F. J. 1993, ApJ, 412, 752 (IR93)
Kawaler, S. D. 1987, PASP, 99, 1322
Kippenhahn, R., & Thomas, H.-C. 1970, in Stellar Rotation, ed. A. Slettebak (Dordrecht: Reidel), 20
Königl, A. 1991, ApJ, 370, L39
Krishna Swamy, K. S. 1966, ApJ, 145, 174
Landin, N. R., Ventura, P., D'Antona, F., Mendes, L. T. S., & Vaz, L. P. R. 2006, in preparation
Linsky, J. L. 1998, Space Sci. Rev., 84, 285
Ludwig, H., Freytag, B., & Steffen, M. 1999, A&A, 346, 111
Ludwig, H.-G., Allard, F., & Hauschildt, P. H. 2002, A&A, 395, 99
Mazzitelli, I. 1989, ApJ, 340, 249
Mazzitelli, I., D'Antona, F., & Caloi, V. 1995, A&A, 302, 382
Mendes, L. T. S., D'Antona, F., & Mazzitelli, I. 1999, A&A, 341, 174
Mihalas, D., Dappen, W., & Hummer, D. G. 1988, ApJ, 331, 815 (M88)
Mohanty, S., Jayawardhana, R., & Basri, G. 2005, ApJ, 626, 498
Montalbán, J., D'Antona, F., Kupka, F., & Heiter, U. 2004, A&A, 416, 1081
Montalbán, J., & D'Antona, F. 2006, MNRAS, in press
Morel, P., van't Veer-Menneret, C., Provost, J., et al. 1994, A&A, 286, 91
Moss, D. L. 1968, MNRAS, 141, 165
Palla, F., & Stahler, W. S. 1990, ApJ, 360, L47
Palla, F., & Stahler, W. S. 1993, ApJ, 418, 414
Palla, F., & Stahler, W. S. 1999, ApJ, 525, 772
Rogers, F. J., Swenson, F. J., & Iglesias, C. A. 1996, ApJ, 456, 902 (R96)
Siess, L., & Livio, M. 1997, ApJ, 490, 785
Soderblom, D. R., Jones, B. F., Balachandran, S., et al. 1993, AJ, 106, 1059
Stahler, S. W. 1988, ApJ, 332, 804
Stassun, K. G., Mathieu, R. D., Mazeh, T., & Vrba, F. J. 1999, AJ, 117, 2941
Stassun, K. G., Ardila, D. R., Basri, G., & Mathieu, R. D. 2004, AJ, 127, 3537
Strom, K. M., Strom, S. E., Edwards, S., Cabrit, S., & Skrutskie, M. F. 1989, AJ, 97, 1451
Trampedach, R., Stein, R. F., Christensen-Dalsgaard, J., J., & Nordlund, Å. 1999, in Theory and tests of convection in stellar structure, ASP Conf. Ser., 173, 233
Tout, C. A., Livio, M., & Bonnell, I. A. 1999, MNRAS, 310, 360
Ventura, P., Zeppieri, A., Mazzitelli, I., & D'Antona, F. 1998, A&A, 331, 1011
Walter, F. M. 1987, PASP, 99, 31